Dual-frequency Spaceborne Doppler Radar: analysis of performances in estimating latent heat fluxes

Simone Tanelli[a] , Jonathan P. Meagher[a], Eastwood Im[a] , Luca Facheris[b]

[a] Jet Propulsion Laboratory, California Institute of Technology, Pasadena CA, USA
[b] Dipartimento di Elettronica e Telecomunicazioni, Università di Firenze, Firenze, Italy

ABSTRACT

Knowledge of the global distribution of the vertical velocity of precipitation is important for estimating latent heat fluxes, and therefore in the general study of energy transportation in the atmosphere. Such knowledge can only be acquired with the use of spaceborne Doppler precipitation radars. Recent studies have shown that the average vertical velocity can be measured to acceptable accuracy levels by appropriate selection of radar parameters. Furthermore, methods to correct for specific errors arising from Non-Uniform Beam Filling effects and pointing uncertainties have recently been developed.
As detailed in the Global Precipitation Mission (GPM) preparatory studies, the use of a dual-frequency precipitation radar allows improved estimation of the main parameters of the hydrometeor size distribution (bulk quantity and one shape parameter). Such parameters, in turn, lead to improved estimates of latent heat fluxes. In this paper we address the performance of a dual- frequency Doppler Precipitation Radar (DDPR) in estimating the latent heat fluxe from the measured rainfall vertical velocity and DSD parameters.

Keywords: Spaceborne precipitation radar, Doppler

1. INTRODUCTION

The heating inside precipitating cloud systems plays a major role in defining the dynamics of the atmosphere. In particular, several studies showed that determination of the temporal and spatial variations of vertical heating could be a vital aid for numerical weather and climate prediction[1]. In general, the only direct means to obtain the latent heating profile is through knowledge of the vertical velocity field and the ability to classify the precipitation into convective, stratiform and transitioning modes[2]. However, aside from isolated wind profilers, there are currently no systems capable of sampling the vertical component of the wind over any significant spatial extent. It is therefore impossible to validate the vertical-wind assumptions (obtained from cloud models, or vorticity methods applied to ground based Doppler radar data) which are required to characterize convection in synoptic and global atmospheric models.

By design, a Dual-Frequency Doppler Precipitation Radar (DDPR) would detect hydrometeors and estimate their vertical speed, *i.e.*, it would measure the reflectivity and vertical velocity of hydrometeors with a high spatial resolution. In addition, the dual-frequency measurements (at 14 and 35 GHz) can be utilized to estimate the first-order statistics of the raindrop size distribution, this allows one to diagnose the wind divergence and latent heating fields directly from the measurements. However, the technological challenges presented by a DDPR have been, in the past, the main reason of concern for the design of a spaceborne mission. Because of such concerns, no spaceborne Doppler radar for atmospheric observation is yet operating. However, the technology to develop such an instrument has developed significantly in the last ten years and spaceborne Doppler technology for atmospheric radars is now available. In fact, a Doppler Cloud Profiling Radar is currently under study in Japan for an ESA program [3]. In this paper we will address the overall feasibility of a DDPR and will provide the preliminary guidelines to assess its performance in estimating vertical profiles of latent heat.

*Simone Tanelli, Jet Propulsion Laboratory, 4800 Oak Grove Drive MS 300-243, Pasadena, CA 91109, U.S.A. E-mail: simone.tanelli@ jpl.nasa.gov

2. HEATING IN CLOUD SYSTEMS

The atmospheric heating budget equations [4] define the 'apparent heat source' Q_1 and the 'apparent moisture sink' Q_2 averaged over an area A including a generic cloud system:

$$Q_1 = \frac{\partial \overline{s}}{\partial t} + \nabla \cdot \overline{s}\,\overline{\boldsymbol{V}} + \frac{\partial \overline{s}\,\overline{\omega}}{\partial p} = Q_R + L_v(\overline{c} - \overline{e}) + (L_v + L_f)(\overline{d} - \overline{s}_*) + L_f(\overline{f} - \overline{m}) - \nabla \cdot \overline{s'\boldsymbol{V}'} - \frac{\partial \overline{s'\omega'}}{\partial p} \quad (1)$$

$$Q_2 = -L_v\left(\frac{\partial \overline{q}}{\partial t} + \nabla \cdot \overline{q}\,\overline{\boldsymbol{V}} + \frac{\partial \overline{q}\,\overline{\omega}}{\partial p}\right) = L_v(\overline{c} - \overline{e}) + L_v(\overline{d} - \overline{s}_*) + L_v \nabla \cdot \overline{q'\boldsymbol{V}'} + L_v \frac{\partial \overline{q'\omega}}{\partial p}, \quad (2)$$

where s is the dry static energy, t is time, $\nabla \cdot \boldsymbol{V}$ is the wind divergence, p is pressure, ω is the vertical p-velocity (*i.e.*, dp/dt) , Q_R is the heating rate due to radiation, L_v is the latent heat of vaporization, L_f is the latent heat of fusion, q is the specific humidity and c,e,d,s_*,f,m are the rates of condensation, evaporation, deposition, sublimation, freezing and melting, respectively. The overbar represents the horizontal average over the area A, and the prime represents deviation from the average. The heating quantities are often expressed in terms of K/day by dividing them by the specific heat of air c_p (constant pressure). These equations have been applied to several diagnostic budget studies in the last thirty years with the purpose of estimating the mechanisms of heat transfer from a cloud system to the large scale environment.

The first level discrimination of the profiles of latent heating depends on the classification of the precipitating system. In fact, early results showed that the heating profiles in stratiform and convective systems are markedly different. Furthermore, it was found that heating profiles of different stratiform systems are generally consistent with one another and from place to place [5]. In general, the mean vertical velocity is upward above the freezing level and downward below it. The magnitude of such velocities is in the tens of cm/s and the vertical profiles are quite consistent throughout the globe and across the seasons. These velocities are consistent with the studies that predict heating in the upper troposphere (mainly due to latent heat release during condensation and deposition) and cooling in the lower troposphere (absorption of latent heat by melting within the melting layer and evaporation below it).

On the other hand, it was observed that this is not the case for convective systems: not only were the heating profiles of convective precipitation found to vary from place to place [5] but field campaigns have shown[6] that the convective regimes (and their associated heating profiles) change significantly at the same location, in the same season, and even within the same mesoscale system, hence adding further uncertainty to the characterization of convection. Maxima of vertical velocity of several m/s (absolute value) are found sometimes in the lower troposphere and sometimes in the upper troposphere, and the corresponding vertical profiles of latent heating derived from diagnostic studies are markedly different. Part of these inconsistencies is due to different observational methods (not all of them being direct measurements of vertical velocity), but significant differences derive from the actual variability of the characteristics of convection even within the same system. For example, updrafts and downdrafts are often coupled, but the relative intensity and position (i.e., altitude at which they occur and horizontal extent) are very variable. Hence, their contributions to the overall latent heating profile are significantly different, in fact, condensation and freezing result from updrafts while evaporation and melting are associated to downdrafts.

Equation (1) can be reshaped [7] to isolate the contributions from three portions of a large area A that includes a generic Mesoscale Convective System (MCS): the environment (cloud-free, indicated by the subscript e), the stratiform portion of the cloud system (small vertical air motions, indicated by the subscript s) and the convective portion of the cloud system (the convective cells embedded in the stratiform area, indicated by

the subscript-index *i* in order to discriminate each convective cell):

$$\frac{\partial \bar{s}}{\partial t} + \nabla \cdot \bar{s}\bar{\boldsymbol{V}} + \frac{\partial s_e \bar{\omega}}{\partial p} - A_e Q_{\mathrm{Re}} =$$

$$= A_s \left[Q_{Rs} + L_v(\bar{c}_s - \bar{e}_s) + (L_v + L_f)(\bar{d}_s - \bar{s}_{*_s}) + L_f(\bar{f}_s - \bar{m}_s) - \frac{\partial \omega_s}{\partial p}(s_s - s_e) + \frac{\partial A_s}{\partial t}\frac{(s_s - s_e)}{A_s} \right] + \tag{3}$$

$$+ \sum_i A_i \left[\underset{(i)}{Q_{Ri}} + L_v \underset{(ii)}{(\bar{c}_i - \bar{e}_i)} + (L_v + L_f) \underset{(iii)}{(\bar{d}_i - \bar{s}_{*_i})} + L_f \underset{(iv)}{(\bar{f}_i - \bar{m}_i)} - \underset{(v)}{\frac{\partial \omega_{is}}{\partial p}(s_i - s_e)} + \underset{(vi)}{\frac{\partial A_i}{\partial t}\frac{(s_i - s_e)}{A_i}} \right]$$

The six terms in the contribution of each cloudy portion (*i.e.*, inside the square brackets) are: (i) net radiative heating, (ii) latent heat exchange due to condensation and evaporation of hydrometeors, (iii) latent heat exchange due to deposition and sublimation of hydrometeors, (iv) latent heat exchange due to melting and freezing of hydrometeors, (v) convergence of sensible heat flux, (vi) expansion and contraction of the cloud cluster.

The relative importance of each term in the right-hand side of Eq. (3) depends on the size of $A_{cloud} = A_s + \Sigma A_i$ with respect to $A = A_{cloud} + A_e$ and on the assumptions that can be made about the characteristics of the large-scale environment. For example, assuming that A_{cloud} / A is large enough so that the environmental radiation term is not important, the typical assumption for tropical systems is that vertical advection dominates the left hand term and that static energy is almost altitude-invariant. Under these conditions the net heating represented by the right hand side is a direct indication of the vertical motion in the area A [7]. In general, the most relevant terms are the contributions by latent heat absorption/release (ii) and (iii).

A practical approach to estimate the rates of phase change appearing in (ii) and (ii) from remote sensors is to derive them from the vertical variation of the mass flux of hydrometeors. For example the Hydrometeor Heating (HH) algorithm [1, 8] assumes that the rate of change from phase 1 to phase 2 can be written as:

$$p_{1,2} = \left| \frac{\partial F_1(z)}{\partial z} - \frac{\partial F_2(z)}{\partial z} \right| \tag{4}$$

where the subscript indicates the hydrometeors in the corresponding phase and *F(z)* is the mass flux:

$$F(z) = M(z)\left[v_T(z) - w(z)\right] \tag{5}$$

where *M(z)* is the mass content, *w(z)* is the vertical wind velocity (positive upwards) and $v_T(z)$ is the mass weighted average terminal velocity of the hydrometeors. The mass content *M(z)* is routinely estimated through spaceborne radar and/or radiometric measurements of received power. When measurements of vertical velocity are not available *w(z)* is estimated from modeled cloud-scale winds and $v_T(z)$ is derived from estimates of the hydrometeor density and size distribution, in fact:

$$v_T = \frac{\pi\rho}{6M}\int v_t(D) D^3 N(D) dD \tag{6}$$

where $v_t(D)$ is the terminal velocity in still air of an hydrometeor of size *D*, *N(D)* is the particle size distribution, and ρ is the water density. Note that the terminal velocity $v_t(D)$ depends significantly on the hydrometeor kind and density, therefore it is crucial to be able to discriminate the amounts of each hydrometeor type (*e.g.*, rain, snow, graupel, etc.). Furthermore, this approach does not account for the horizontally advected masses of hydrometeors, therefore analysis of the three-dimensional spatial distribution of the hydrometeors is necessary to refine estimates of latent heating profiles.

Perhaps the most systematic effort in providing large-scale estimates of the heating in precipitating systems is that of the Tropical Rainfall Measuring Mission (TRMM). Notably, the TRMM Precipitation Radar (PR) is a Ku-band, non-Doppler radar paired to a multifrequency radiometer (TMI) and other passive sensors. Three algorithms for estimating latent heat have been developed for TRMM: the first is the HH algorithm based of the vertical mass flux analysis described above. Correcting terms are added to account for the mass flux of cloud liquid content and the calibration uncertainties. Since the cloud-scale vertical velocity *w* is not measured by TRMM, an estimated velocity is regressed from the vertical profiles relying on information provided by cloud-resolving model (CRM) simulations. The second is the Convective Stratiform Heating (CSH) algorithm which needs information only on the surface rainfall rate, amount of stratiform rain and the type and location of the observed cloud system. The retrieval of latent heating profiles is obtained through a look up table composed of convective profiles for different regions of the globe and different seasons. The third is the Goddard PROFiling Heating Bayesian algorithm (GPROFH) which retrieves the vertical profiles of latent heating by calculating the weighted-average of CRM-simulated profiles, weighted accordingly to the fit of the corresponding forward simulated radiometric quantities with the measurements.

As recently demonstrated [9], the three algorithms provide estimates of the magnitude of maximum heating rates consistent with each other (4-6 K day^{-1}) and are comparable to those provided by budget studies (4-10 K day^{-1}). On the other hand, several differences are evident in the retrieved vertical profiles and no evidence is yet available to determine which algorithm, if any, performs the best. Among the possible causes for these differences four factors seem to dominate: 1) uncertainties in the estimation of surface rainfall rate, 2) classification of convective vs. stratiform areas, 3) characterization of convection in different portions of the globe and different seasons, 4) impact of different spatial resolution. In general, each of the three algorithms would benefit from measurements of vertical velocity. In fact, such measurements would a) expand the available databases that characterize convection in different portions of the globe (CSH), b) provide a very specific criterion to select a CRM-simulated hydrometeor profile (GPROFH), c) provide direct estimates of vertical velocity (HH), d) improve the reliability of convective/stratiform classification for any given profile (all). Furthermore, estimates of *w* would allow to calculate the wind divergence which would, in turn, provide estimates of the eddy flux contribution in Eq. (1) (which is otherwise ignored), and of the horizontally advected mass fluxes.

3. SPACEBORNE MEASUREMENTS OF MEAN DOPPLER VELOCITY

Recent studies [10,11,12] have focused on the system requirements for a Doppler Precipitation Radar mounted on a Low Earth Orbiting (LEO) spacecraft. It was found that the high linear speed of a LEO satellite causes a significant Doppler shift to the radar echo originated from different portions of the antenna mainlobe. For narrow beam, nadir-looking (or cross-track scanning) radars, such a Doppler shift (in m/s) is roughly proportional to $x\, v_s / h_s$ where x is the along-track displacement of the target with respect to the spacecraft, v_s is the satellite velocity and h_s is the local satellite altitude. If the radar volume of resolution is uniformly filled with hydrometeors, the result is that the natural rainfall Doppler spectrum (determined by the different vertical velocity of the hydrometeors) is broadened by the additional 'spacecraft-motion' Doppler shift. The observed Doppler spectrum is approximately Gaussian (provided that the pattern of the antenna mainlobe is approximately Gaussian) with normalized spectral width:

$$w_N = \frac{2}{\lambda PRF}\sqrt{\sigma_R^2 + \frac{\theta_{3dB}^2 v_S^2}{16\ln(2)}} \tag{7}$$

where λ is the operating wavelength, *PRF* is the Pulse Repetition Frequency, θ_{3dB} is the antenna 3-dB width, and σ_R is the spread in hydrometeor vertical velocity due to different size, turbulence and wind shear.

σ_R	Ku band (13.6 GHz)							Ka band (35 GHz)						
	D_a	2	3	4	5	6	10	D_a	2	3	4	5	6	10
	θ_{3dB} / PRF	.76	.51	.38	.30	.25	.15	θ_{3dB} / PRF	.29	.20	.15	.12	.10	.06
1	5000	**.50**	**.34**	**.25**	**.20**	**.17**	**.10**	5000	**.51**	**.34**	**.26**	**.21**	**.17**	**.11**
	6000	**.42**	**.28**	**.21**	**.17**	**.14**	**.09**	6000	**.42**	**.28**	**.21**	**.17**	**.15**	**.09**
	7000	**.36**	**.24**	**.18**	**.14**	**.12**	**.07**	7000	**.36**	**.24**	**.18**	**.15**	**.12**	**.08**
	8000	**.32**	**.21**	**.16**	**.13**	**.11**	**.06**	8000	**.32**	**.21**	**.16**	**.13**	**.11**	**.07**
3	5000	**.51**	**.34**	**.26**	**.21**	**.18**	**.11**	5000	**.52**	**.36**	**.29**	**.25**	**.22**	**.17**
	6000	**.42**	**.28**	**.22**	**.17**	**.15**	**.10**	6000	**.44**	**.30**	**.24**	**.20**	**.18**	**.14**
	7000	**.36**	**.24**	**.18**	**.15**	**.13**	**.08**	7000	**.37**	**.26**	**.21**	**.18**	**.16**	**.12**
	8000	**.32**	**.21**	**.16**	**.13**	**.11**	**.07**	8000	**.33**	**.23**	**.18**	**.15**	**.14**	**.11**
5	5000	**.51**	**.35**	**.27**	**.22**	**.19**	**.14**	5000	**.56**	**.41**	**.34**	**.31**	**.29**	**.25**
	6000	**.43**	**.29**	**.22**	**.18**	**.16**	**.11**	6000	**.46**	**.34**	**.29**	**.26**	**.24**	**.21**
	7000	**.37**	**.25**	**.19**	**.16**	**.14**	**.10**	7000	**.40**	**.29**	**.25**	**.22**	**.21**	**.18**
	8000	**.32**	**.22**	**.17**	**.14**	**.12**	**.08**	8000	**.35**	**.26**	**.21**	**.19**	**.18**	**.16**

Table 1: Normalized Doppler spectral widths as function of operating wavelength, antenna diameter, Pulse Repetition Frequency and turbulence regime.

The normalized Doppler spectral widths that correspond to several system configurations and regimes of turbulence are described in Table 1. The category of moderately broad spectra (*i.e.*, $0.1 < w_N < 0.3$) that can be obtained with antenna sizes $D_a < 10$ m is suitable only for estimation of the first spectral moment [13], (i.e, the mean, backscattering weighted, Doppler velocity) and the variance of such estimate can be expressed as:

$$\mathrm{var}(\hat{v}_P) = \frac{\lambda^2 PRF^2}{4M_S}\left[\frac{w_N}{4\sqrt{\pi}} + 2w_N^2\,\frac{S_N}{S_S} + \frac{1}{12}\left(\frac{S_N}{S_S}\right)^2\right] \tag{8}$$

where M_S is the number of samples, S_S is the signal power and N_S is the noise power. Several possibilities are available, in principle, to remove the effect of the Doppler shift (*e.g.*, operation from a geostationary platform, or use of a dual antenna on a LEO satellite, use of a very large antenna on a LEO satellite), however they all present further technological challenges and will not be addressed in this paper.

If the radar volume of resolution is not homogeneously filled with hydrometeors (*i.e.*, in Nonuniform Beam Filling conditions, NUBF) the uneven weighting of the Doppler shift in different portions of the mainlobe causes the observed Doppler spectrum[14] to be asymmetric around the mean Doppler velocity and can introduce a bias of several m/s in vertical velocity measurements. The Combined Frequency Time (CFT) spectral processing technique proposed in [15] is able to remove such NUBF-induced bias provided that several spectra are measured on volumes of resolution partially overlapping in the along-track direction. A further advantage of adopting CFT is that the along-track horizontal resolution is improved to the distance covered by the spacecraft between consecutive spectra (in the notional configuration considered in that study this corresponds to approximately 75 m). On the other hand, the price for such high quality information at one specific scan angle is that limited resources are left for cross-track scanning. Preliminary trade-off studies show that configurations with 3 or 5 beams per cross-track scan could be used together with CFT, but performance degrades rapidly if that number is further increased. In general, it was shown[15] that an accuracy of <1 m/s can be achieved with a Doppler Precipitation Radar configuration with a 3 to 6 m antenna size. Such accuracy can be obtained over homogeneous rainfall fields through standard spectral moment estimators (such as Pulse Pair processing or Fourier-based Spectral Analysis), or through CFT in more general NUBF conditions.

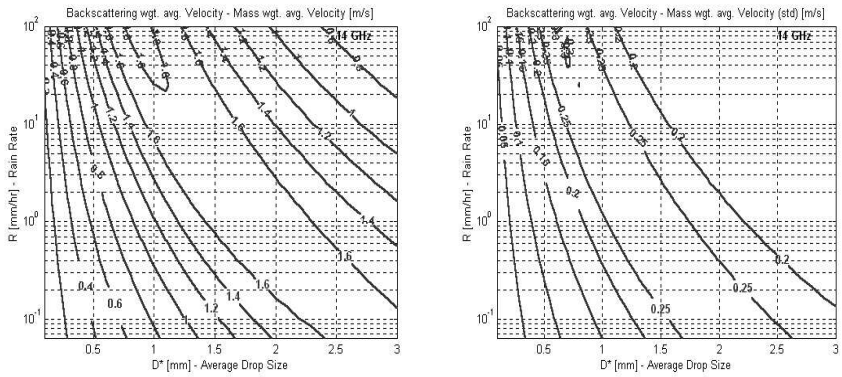

Figure 1 – Offset between backscattering weighted and mass weighted mean Doppler velocity. The parametrization of N(D) is the one proposed in [21] : R, D'' (= $D_m R^{-0.155}$) and s'' (= $s_m D_m^{-0.165} R^{-0.0114}$). a) bias calculated for s"=0.38, b) standard deviation of the offset for all s".

For a near nadir pointing angle, the measured Doppler velocity is the reflectivity weighted velocity of the hydrometeors:

$$v_P = \frac{1}{\eta}\int v_p(D)\sigma_b(D)N(D)dD \tag{9}$$

where $\sigma_b(D)$ is the backscattering cross-section of a hydrometeor of diameter D, $v_p(D)$ is its vertical velocity ($v_p(D) = v_t(D) - w$), and η is the radar reflectivity. The velocity v_P is related to the two more physically meaningful quantities discussed in Section 2: the vertical wind speed w and the mass-weighted mean Doppler velocity v_M=v_T-w. The problem of estimating w and v_M from v_P measurements is related to the estimation of $N(D)$. Assuming for example that $N(D)$ is Gamma distributed with mean (mass weighted) drop diameter D_m and normalized standard deviation s_m, the relation between v_P and v_T is described in Figure 1. Assuming an uncertainty of 0.2 mm on D_m and no information on s_m, one can estimate v_T from v_P with an uncertainty smaller than <0.5 m/s.

Several techniques have been developed to estimate the first-order moments of $N(D)$ from radar and radiometric measurements. While it is possible to envisage the combined use of a DDPR with radiometers (as it has been done with non-Doppler systems on TRMM and in the planning of GPM), we focus on the use of Dual-frequency radar measurements in order to simplify the problem to simultaneous, multiparametric measurements with identical spatial resolution. In general, dual-frequency radar measurements rely on the fact that Mie scattering must be accounted for in modeling the e.m. characteristics of hydrometeors at operating frequencies above 5 GHz. It follows that the shape of $\sigma_b(D)/\eta$ changes depending on the operating frequency and D_m can be estimated from dual-frequency radar measurements.

4. ESTIMATION OF HEATING PROFILES WITH DOPPLER RADAR MEASUREMENTS

In this section we describe three contributions that simultaneous measurements of dual-frequency reflectivity (Z_{m1},Z_{m2}) and mean Doppler velocity (v_P) can bring to the goal of estimating the heating associated with cloud systems.

4.1 CONVECTIVE/STRATIFORM CLASSIFICATION

As mentioned above, the distribution of heating in the stratiform precipitation areas is considerably different from the vertical profile of heating in the convective regions. As a matter of fact, it is suggested [9] that inconsistencies in the estimation of the convective portion of a rainfall system might be one of the leading sources of error in large scale estimates of vertical profiles of heating.

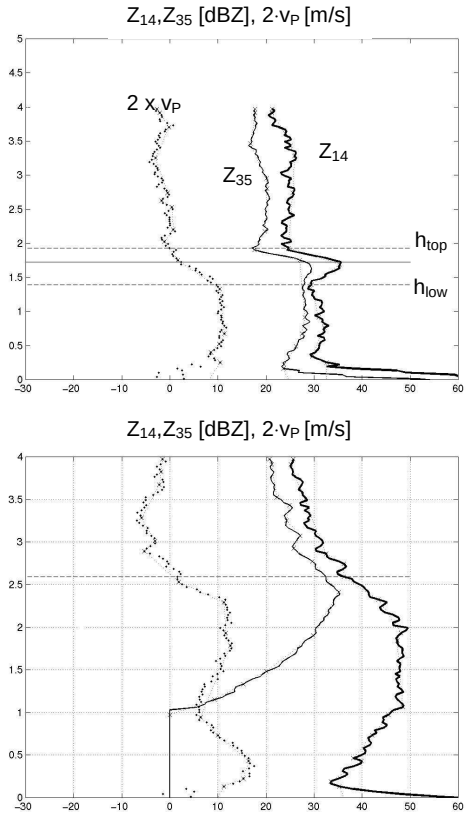

Figure 2: Classification of profiles (Jan 19th, 2003 Wakasa Bay Ex.). a) Stratiform case, melting layer detected between 1.4 and 2 km altitude; b) Convective case, updraft above 0.5 km altitude.

Stratiform precipitation is generally characterized by little or no vertical air motion (*i.e.*, $|w| << 1$ m/s) and by the presence of a well defined melting layer of 0.3 to 1 km thickness which is associated to a brightband signature in the radar reflectivity. Spaceborne precipitation radars such as TRMM/PR are already recognized as the optimal tool to discriminate between stratiform systems, convection and other precipitation types. This is mainly due to their higher spatial (horizontal and vertical) resolution as compared to passive sensors. While the performances of the classification are satisfactory [17], some inconsistencies are observed. Furthermore, the extension of the observed latitudinal region from TRMM to GPM will preclude the usage of some a priori conditions on the altitude of the brightband used in the current TRMM algorithm for the detection of the brightband. In fact, the TRMM classification algorithm [16] assumes that the brightband is within a predetermined altitude range (an assumption consistent with the tropical latitudes), and that presence of reflectivities of 40 dBZ or higher below the freezing level are always associated with convection, (which is true in the tropics but has been demonstrated to be not always true over the globe, see for example a study performed in Montreal that showed that nearly half of the events with radar reflectivity in the 40-45 dBZ range was resulting from non convective rain [18]).

We have recently developed a multiparametric radar brightband detection algorithm [19] that makes use of dual-frequency reflectivity (14 and 35 GHz) and mean Doppler velocity measurements. The algorithm first determines an approximate altitude of the melting layer by averaging vertical velocity profiles over an area of several km (in order to reduce the relative contribution of convective profiles). In stratiform areas, the averaged velocity profile has a typical step-like shape determined by the higher falling speed of liquid hydrometeors vs. low density frozen hydrometeors (*i.e.*, $v_P \sim 1$ m/s above the melting layer and $v_P > 4$ m/s below it). A first-guess of the freezing level altitude is set at 500 meters above the point where the average velocity profile reaches its maximum. The algorithm proceeds on a profile-by-profile basis, by finding the typical sharp increase in reflectivity measurements that occurs where the frozen hydrometeors begin to melt. Such a sharp increase is searched for at altitudes within a 1.5 km range from the first-guess and it is associated with the top of the melting layer (h_{top}). The reliability of the detection of h_{top} is significantly improved when both reflectivity profiles are analyzed together. This is due to the fact that any sharp increase in reflectivity due to the beginning of the melting process must show a well defined and predictable correlation between the two frequencies. Finally the negatively correlated variations of reflectivity at 14 GHz and v_P are analyzed starting from the top of the melting layer to determine the bottom of the melting layer (h_{low}). In fact, in the lower part of the melting layer the reflectivity at 14 GHz drops and the mean Doppler velocity increases because the hydrometeors increase their density (hence reducing their size and number density – the latter because of the acceleration to a faster terminal velocity). The reflectivity profile at 35 GHz is not used in the determination of h_{low} because the deeper Mie scattering regime at 35 GHz is

such that the reduction in average particle size does not always result in correspondingly lower reflectivities. The algorithm was first developed for the measurements obtained by the NASA/JPL airborne, dual-frequency, dual-polarization, Doppler radar APR-2 [20] and therefore also the vertical profiles of Linear Depolarization Ratio can be used to refine the estimation of h_{low}. It was found that, if no cross-polarimetric measurements are available, the algorithm simply underestimates by <10% the melting layer thickness if measurements are obtained at the vertical resolution of 30 m (APR-2 radar resolution). A spaceborne atmospheric radar is in general designed to have a vertical resolution of 250m or more for increased sensitivity, that is, significantly larger than this underestimation which can be therefore ignored in first approximation. Overall the algorithm was found to provide extremely reliable estimates of the presence, altitude and thickness of the melting layer without the a priori information currently used in non-Doppler algorithms.

Profiles that do not show a brightband and whose vertical velocity profile does not correlate with the vertical velocity profile of the surrounding stratiform rain are classified as convective. Profiles with no brightband but with vertical velocity consistent with the stratiform ones are classified as other. The convective vs. stratiform classification is thus obtained with no need for analyzing also the horizontal patterns of reflectivity (as in TRMM classification algorithm).

4.2 ESTIMATION OF SURFACE RAINFALL

The basis for the simplest approach to the estimation of latent heating is based on the fact that a mass conservation approach[4] applied to a vertical profile shows that the total heating released by a column within a precipitating system is roughly equivalent to the liquid water mass flux exiting the column multiplied by the specific latent heat of vaporization of water (L_v). Assuming that no horizontal advection is present, one can approximate the mass flux by the surface rainrate. Furthermore, at low altitudes (*i.e.*, within the boundary layer) the average vertical wind over an area of few km^2 is negligible. Therefore, the 'still-air' rainfall rate R typically obtained by rain retrieval algorithms is a good estimator of the total heating.

Several groups of algorithms are used to estimate R from non-Doppler spaceborne systems (single and dual frequency radar, multifrequency radiometric or radar/radiometer combined algorithms). In principle, one can modify any of them to exploit the information provided by Doppler measurements of average vertical velocity. Most of the retrieval algorithms aim at estimating the rain rate (R) and the mean drop diameter. The contribution of v_P measurements to this goal is best seen by adopting the DSD parametrization proposed in [21] for the gamma distribution: R is the rain rate estimated in still air, D'' is a parameter proportional to D_m and s'' is proportional to s_m. The advantage of these three parameters is that they are almost statistically independent.

In order to assess the contribution of Doppler measurements to the rainfall inversion problem, Figure 3 shows the value of two Jacobian determinants: J_{ZV} is calculated assuming that the observables are the radar reflectivity (in dBZ) at 14 GHz Z_{14} and v_P, J_{ZZ} is calculated assuming that the observables are the two radar reflectivities Z_{14} and Z_{35}. In both cases the independent variables are the $10*log_{10}(R)$ and D''. In the region of high rain rates and large

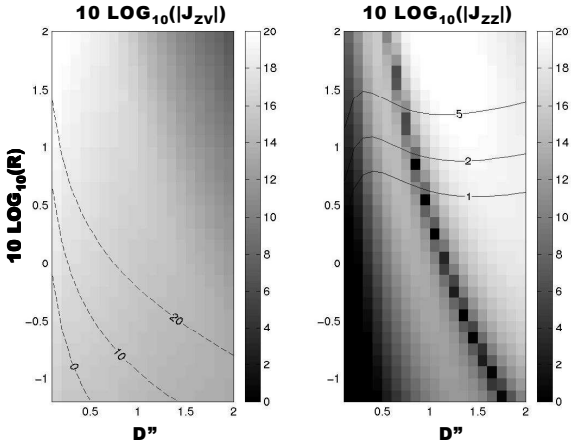

Figure 3 – Jacobian determinants J_{ZV} and J_{ZZ} in the R-D'' space. The dashed and solid isopleths represent Z_{14} (dBZ) and specific attenuation at Ka band (dB/km), respectively.

drops (*i.e.*, where Mie scattering dominates Ka band measurements) large values of J_{ZZ} indicate that the pair (Z_{14},Z_{35}) is almost independent. On the other hand, since for large drops the average terminal velocity is not very sensitive to changes in drop diameter, one has smaller values of J_{ZV}. In this area however one must account also for the large attenuation that occurs at Ka band and therefore the pair (Z_{14},Z_{35}) is in general usable only for $R < 15$ mm/hr. At the other side of the R-D'' space (*i.e.*, for small D'' and small R), the low value of J_{ZZ} is due to the fact that Rayleigh scattering dominates at both frequencies and therefore no additional information is provideded by Z_{35} with respect to Z_{14}. On the other hand, J_{ZV} shows significantly larger values due to the high sensitivity of v_P to changes in mean drop diameter. Note that, for very small R and D'', in principle the pair (Z_{14}, v_P) delivers enough information to retrieve accurately the rainfall parameters. However, the corresponding SNR at Ku band can be very low (*e.g.*, compare the dashed curves indicating the radar reflectivity in the left panel with TRMM/PR sensitivity of 17dBZ), thus degrading the accuracy of v_P estimates. Considering that the use of Ka band allows to reach better sensitivities, one might use the pair (Z_{35}, v_P) in order to extend further the range of measurable rain conditions. However, in this case, the trade-off study for the system design must account for the fact that imposing 'matching beams' implies that Doppler spectra at Ka band are roughly 2.5 times broader than those at Ku band.

4.3 HYDROMETEOR HEATING METHOD

Estimates of vertical heating profiles through the HH algorithm are sensitive to the correct classification of the phase of hydrometeors. As described in Section 4.1, such discrimination is easily obtained by a DDAR on stratiform areas, or more generally, when no significant vertical wind is present. Furthermore, the improved estimates of rainrate and D_m described in section 4.2 result in general in accurate profiles of latent heating. On the other hand, in convective areas (*i.e.*, where w is not negligible), frozen and liquid particles can be discriminated only by dual-frequency reflectivity measurements (which rely on the fact that the specific attenuation of frozen particles is markedly smaller than that of liquid hydrometeors) and, similarly, their bulk quantities and mean diameters cannot be improved through Doppler measurements. Even assuming that the hydrometeor type, bulk quantity, and mean diameters are well estimated by the dual-frequency measurements, further uncertainty in estimating the mass-flux $F(z)$ is introduced in Eq. (5) by convective updrafts and downdrafts if measurements of vertical velocity are not available. On the other hand, the average (mass weighted) vertical velocity v_M can be estimated from measurements of v_P with an error smaller than the threshold that defines whether convection is present or not.

The performances of DDPR in estimating the latent heating of a precipitating system have been analyzed through simulations. The case study shown in Figure 4 is obtained from a CRM generated tropical storm showing a very strong convective cell at km 20 and a weaker one at km 30 (see panel e for bulk quantities of rain and graupel, panel f for the corresponding mass-fluxes and panel c for the hydrometeor vertical velocity). The area between km 10 and km 20 is a stratiform area 'fed' mainly by the first convective cell. The strong updraft of cell 1 occurs between 3 and 15 km altitude and is connected with a high-level downdraft around km 13 altitude and a low-level downdraft below 4 km altitude. The DDPR measurements were simulated through a three-dimensional Doppler radar simulator[14] and the CFT technique[15] was applied to retrieve v_P . The DDPR was configured as follows: not-scanning (nadir-looking only), PRF = 7kHz, antenna size 5m with matching beams (Ka band using only 40% of the antenna size), pulse duration 1.6 μs and 64 samples per spectrum (corresponding to a 240 m vertical resolution and along-track sampling rate of 1/64 m^{-1}). The simulated reflectivities Z_{14} and Z_{35} are shown in panels a and b, respectively, and the CFT retrieved v_P is shown in panel d. Panels g and h show latent heating estimates obtained through an adapted version of the HH algorithm: in this version only the heating from precipitating hydrometeors is calculated. In panel g, the mean terminal velocities are obtained through hydrometeor-specific M-v_T relations and no vertical wind is assumed (HH0). In panel h, the mass flux is obtained by estimating v_M from the v_P measurements as described in section 2 (HHV).

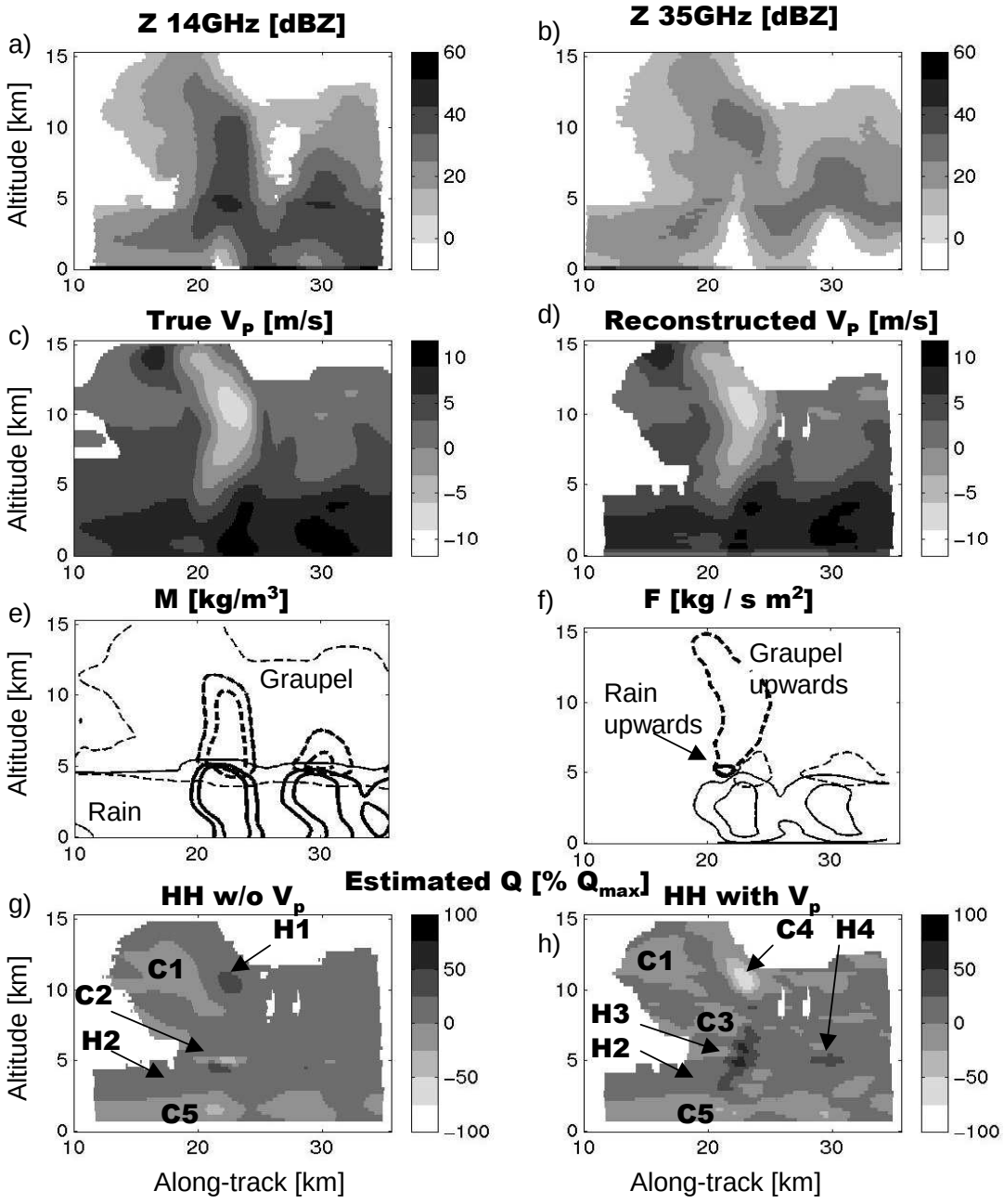

Figure 4: DDPR simulated measurements of a CRM-generated tropical storm. a) Measured Ku band reflectivity, b) measured Ka band reflectivity, c) True vertical velocity of the hydrometeors, d) Hydrometeors vertical velocity estimated by DDPR through CFT technique, e) Mass content of graupel (dashed) and rain (solid) , thin = 0.01 kg/m^3 , thick = 1 and 3 kg/m^3 , f) Vertical mass flux, thick = upwards, thin = downwards, g) Latent heating field estimated through HH without Doppler measurements (Q_{max}=165 K/hr), h) Latent heating field estimated through HH with Doppler measurements.

The retrieved latent heating fields were compared to the latent heating field generated by the CRM. While both retrievals are in good agreement (*i.e.*, within 20%) with the model on the column integrated latent heating, significant differences occur in the vertical profiling. The along-track averaged vertical profile generated by the CRM has a maximum peak of 30 K/hr at 5 km altitude which is retrieved correctly by HHV while HH0 has the maximum of 23 K/hr at 4.5 km. Also, the HHV profile shows a high-level cooling of –10 K/hr at 12 km altitude in agreement with the CRM-generated profile, while HH0 does not detect it. Both algorithms fail to detect a second peak of 25 K/hr heating at 8 km altitude and overestimate the low level cooling (-12 K/hr instead of –4 K/hr). These differences can be understood by accounting for the features in the heating field indicated in panels g and h. The cooling areas C3 and C4, and the heating areas H3 and H4 visible in panel h are in good agreement with the CRM-generated latent heating field. Note that C4 is erroneously replaced by H1 in the HH0 retrieval, H3 is significantly underestimated and partially replaced by the cooling C2 due to a non-existing melting layer (updraft region corresponding to re-freezing instead, see panel e), and C3 and H4 are also lost in the HH0 retrieval. The weak high-level cooling C1 is overestimated by both algorithms, and the low level heating H2 below the melting layer of the stratiform region corresponds to a region of weak cooling in the model, also the low level cooling C5 in the lower part of both convective cells is not present in the model. The cause for the errors relative to C5 and H2 has been clearly identified as the contribution of horizontal advection.

5. CONCLUSIONS

The results of a preliminary study on the performance of a Dual-Frequency Doppler Precipitation radar in estimating the vertical profiles of latent heat in a precipitating system are presented in this paper. The results of simulations show that the availability of measurements of vertical velocity of the hydrometeors with the 1 m/s accuracy achievable with the current technology by a spaceborne Doppler radar would allow direct estimation of the vertical profiles of latent heat release and absorption.

ACKNOWLEDGMENTS

The research described in this paper was based on the work performed for the Tropical Rainfall Measuring Mission (TRMM) and the Global Precipitation Measurements (GPM) programs at the Jet Propulsion Laboratory, California Institute of Technology, under contract with the National Aeronautics and Space Administration, and at the University of Florence (Italy) through a program funded by the Italian Space Agency.

REFERENCES

1 S. Yang, and E. A. Smith, “Moisture budget analysis of TOGA COARE area using SSM/I-retrieved latent heating and large scale Q_2 estimates”. *J. Atmos. Ocean. Tech.*, **16**, 633-655, 1999.

2 R. A. Houze Jr., S. G. Geotis, and F. D. Marks, “Stratiform precipitation in regions of convection: a meteorological paradox”. *B. Am. Meteorol. Soc.*, **78**, 2179-2196, 1997.

3 European Space Agency, ”EarthCare-Earth Clouds, Aerosols and Radiation Explorer”. ESA Publication Division, 130 pp, 2001.

4 M. Yanai, S. Esbensen, and J. Chu, ”Determination of average bulk properties of tropical cloud clusters from large-scale heat and moisture budgets”. *J. Atmos. Sci.*, **30**, 611-627, 1973.

5 R. A. Houze Jr., “Observed structure of mesoscale convective systems and implications for large-scale heating”. *Q. J. Roy. Meteor. Soc.*, **115**, 425-461, 1989

6 R. Cifelli, L. Carey, W. A. Petersen, and S. A. Rutledge, “An ensemble study of wet season convection in the south west amazon: kinematics and implications for diabatic heating”, *Proc. of the 31st Conf. On*

Radar Met., Seattle Aug. 6-12 2003, 391-394, 2003.

7 R. A. Houze Jr., "Cloud clusters and large-scale vertical motions in the tropics", *J. Meteorol. Soc. Japan*, **60**, 396- 409, 1982.

8 W. K. Tao, S. Lang. J. Simpson, and R. Adler, "Retrieval algorithms for estimating the vertical profiles of latent heat release: their applications for TRMM", *J. Met. Soc. of Japan*, **71**, 685-700, 1993.

9 W. K. Tao, S. Lang, W. S. Olson, R. Meneghini, S. Yang, J. Simpson, C. Kummerow, E. A. Smith, and J. Halverson, "Retrieved vertical profiles of latent release using TRMM rainfall products for February 1998", *J. App. Met.*, **40**, 957-982, 2001.

10 R. Meneghini and T. Kozu, "Spaceborne Weather Radar", Artech House, 201 pp, 1990.

11 P. Amayenc, J. Testud, and M. Marzoug, "Proposal for a spaceborne dual-beam rain Radar with Doppler capability", *J. Atmos. Oceanic Technol.*, **10**, 262-276, 1993.

12 S. Tanelli, E. Im, S. L. Durden, and L. Facheris, "System and Performance Analyses of Spaceborne Doppler Radars for Measuring Vertical Rainfall Velocity", *Proc. of the 83rd AMS Annual Meeting, Feb 9-13 2003, Long Beach CA, USA*. (CD-ROM, Paper # 1.2 in 7th Symp. on Integrated Observing Systems: The water cycle), 2003.

13 S. Tanelli, Eastwood Im, Luca Facheris, and Eric A. Smith, "DFT-based spectral moment estimators for spaceborne Doppler precipitation radar", *Proc. of SPIE*, **4894**, SPIE Symposium on Remote Sensing of the Atmosphere, Environment and Space, Hangzhou (RPC), Oct. 23-27 2002.

14 S. Tanelli, E. Im, S. L. Durden, L. Facheris, and D. Giuli, "The effects of nonuniform beam filling on vertical rainfall velocity measurements with a spaceborne Doppler radar", *J. Atmos. Oce. Technol.*, **19**, 1019-1034, 2002.

15 S. Tanelli, E. Im, S. L. Durden, L. Facheris, D. Giuli, and E. A. Smith, "Rainfall Doppler velocity measurements from spaceborne radar: overcoming nonuniform beam filling effects". *J. Atmos. Oce. Technol.*, in press (2003).

16 J. Awaka, T.Iguchi, H.Kumagai, and K.Okamoto, "Rain Type classification algorithms for TRMM Precipitation Radar", *Proc. of IGARSS'97*, 3-8 Aug. 1997, 1633-1635, 1997.

17 S. L. Durden, E. Im, Z. S. Haddad, and L. Li, "Comparison of TRMM Precipitation Radar and Airborne Radar Data", *J. App. Met.*, **42**, 769-774, 2003.

18 F. Fabry, and I. Zawadzki, "Long-term radar observations of the melting layer of precipitation and their interpretation". *J. Atmos. Sci.*, **52**, 838-851, 1995.

19 S. Tanelli, J. P. Meagher, S. L. Durden, and E. Im, "Multiparametric airborne radar observations of the melting layer during the Wakasa Bay Experiment", *Proc. of the 31st Conf. on Radar Met.*, Seattle Aug. 6-12 2003, 33-34, 2003.

20 G. A. Sadowy, A. C. Berkun, W. Chun, E. Im, and S. L. Durden, "Development of an advanced airborne precipitation radar", *Microwave Journal*, **46**, 2003.

21 Z. S. Haddad, D. A. Short, S. L. Durden, E. Im, S. Hensley, M. B. Grable, and R. A. Black, "A new parametrization for the rain drop size distribution", *IEEE Trans. Geosc. Rem. Sens.*, **35**, 532-539, 1997.